ORIGINAL PAPER

EEG Microstates as Markers for Cognitive Impairments in Fragile X Syndrome

Yukari Takarae[1,2] · Anthony Zanesco[3] · Craig A. Erickson[4,5] · Ernest V. Pedapati[4,5,6]

Abstract
Fragile X syndrome (FXS) is one of the most common inherited causes of intellectual disabilities. While there is currently no cure for FXS, EEG is considered an important method to investigate the pathophysiology and evaluate behavioral and cognitive treatments. We conducted EEG microstate analysis to investigate resting brain dynamics in FXS participants. Resting-state recordings from 70 FXS participants and 71 chronological age-matched typically developing control (TDC) participants were used to derive microstates via modified k-means clustering. The occurrence, mean global field power (GFP), and global explained variance (GEV) of microstate C were significantly higher in the FXS group compared to the TDC group. The mean GFP was significantly negatively correlated with non-verbal IQ (NVIQ) in the FXS group, where lower NVIQ scores were associated with greater GFP. In addition, the occurrence, mean duration, mean GFP, and GEV of microstate D were significantly greater in the FXS group than the TDC group. The mean GFP and occurrence of microstate D were also correlated with individual alpha frequencies in the FXS group, where lower IAF frequencies accompanied greater microstate GFP and occurrence. Alterations in microstates C and D may be related to the two well-established cognitive characteristics of FXS, intellectual disabilities and attention impairments, suggesting that microstate parameters could serve as markers to study cognitive impairments and evaluate treatment outcomes in this population. Slowing of the alpha peak frequency and its correlation to microstate D parameters may suggest changes in thalamocortical dynamics in FXS, which could be specifically related to attention control. (250 words)

Keywords EEG Microstates · Fragile X Syndrome · Resting-State Networks · Alpha Power · Intellectual Disabilities

Communicated by Christoph Michel

✉ Yukari Takarae
ytakarae@ucdavis.edu

1 Department of Psychiatry and Behavioral Sciences, University of California, Davis, Sacramento, CA, USA

2 M.I.N.D. Institute, University of California, Davis, Sacramento, CA, USA

3 Department of Psychology, University of Miami, Coral Gables, FL, USA

4 Division of Child and Adolescent Psychiatry, Cincinnati Children's Hospital Medical Center, Cincinnati, OH, USA

5 Department of Psychiatry, University of Cincinnati College of Medicine, Cincinnati, OH, USA

6 Division of Neurology, Cincinnati Children's Hospital Medical Center, Cincinnati, OH, USA

Introduction

Fragile X syndrome (FXS) is one of the most common causes of inherited intellectual disabilities (Verkerk et al. 1991). FXS is a trinucleotide repeat disorder in which the CGG repeat in the untranslated region of the Fragile X Messenger Ribonucleoprotein 1 (FMRP1) gene is abnormally expanded, which yields reduced production of Fragile X Messenger Ribonucleoprotein (FMRP) (Bagni et al. 2012; Verkerk et al. 1991). FMRP is an RNA-binding protein that is essential in regulating local protein synthesis and normal cell functions, and thus, it is critical for cognitive function (Bagni et al. 2013, Garber et al. 2008). The average intellectual quotient (IQ) in FXS is approximately 40–45 compared to the normed average of 100 in the general typically developing population (Sansone et al. 2014). Comorbidity with autism is common, and the reported prevalence rates range from 15 to 60% (Budimirovic et al. 2011). Anxiety

and attention deficit disorders are also frequently observed in FXS (Boyle et al. 2010).

While there is currently no cure for FXS, treatments to help ameliorate behavioral problems are actively developed and tested, and EEG is considered an important tool for understanding the pathophysiology of FXS and the mechanisms underlying effects of treatment. Past studies have reported several differences in EEG characteristics of FXS individuals relative to control participants, including enhanced amplitudes of ERP responses (Ethridge et al. 2019, Knoth et al. 2012) and elevated gamma power combined with reduced phase-locking (Ethridge et al. 2017; Pedapati et al. 2022; Wang et al. 2017). The peak alpha frequency has been reported to be lower than control participants (Pedapati et al. 2022; Smith et al. 2021, Van der Molen et al. 2013) with reduced alpha-gamma coupling accompanied by increased theta-gamma coupling (Wang et al. 2017).

The current study examined EEG microstates at rest in a large sample of individuals with FXS and control participants. EEG microstates are defined based on the topography of the scalp electric field. Each microstate represents a brief period in which the scalp topography remains quasi-stable (40–120 ms) (Lehmann 1971), resulting from the transient co-activation of underlying neural generators. Consequently, each change in the scalp topography of a microstate signifies a change in the sets of neural generators (Lehmann et al. 1987; Vaughan 1982). Thus, EEG microstates capture non-stationary global activity patterns that reflect activities of distinct, widely distributed networks (Khanna et al. 2015, Michel et al. 2018). EEG microstate analysis can therefore complement past ERP and spectral studies that emphasize average signal characteristics over time. To our knowledge, this is the first study on EEG microstates in FXS.

Each microstate is considered to represent a specific global brain state that has functional relevance for cognition. For instance, microstates show orderly transitions that correspond to cognitive states that are experienced by participants (Pipinis et al. 2017; Zanesco et al. 2021a). Different microstates are observed during visual and verbal processing (Lehmann et al. 1998, 2010; Milz et al. 2016). Microstates observed during the pre-stimulus period predict performance on cognitive tasks, including accuracy and error (Britz et al. 2010a, Britz et al. 2014) and reaction time (Zanesco et al. 2020a). The prominence of certain microstates also has been reported to change by arousal levels or sleepiness (Comsa et al. 2019). The suggested neural sources for EEG microstates include key structures of resting-state fMRI networks, such as the default mode, attention, and salience networks (Bréchet et al. 2020; Britz et al. 2010b; Custo et al. 2017; Musso et al. 2010; Yuan et al. 2012). Further, EEG microstates have been shown to predict fluctuations in fMRI dynamic functional connectivity with 90% accuracy (Abreu et al. 2020).

Past studies have shown that microstate temporal parameters (e.g., duration and occurrence) are altered in several clinical conditions, including autism, schizophrenia, and dementia (Al Zoubi et al. 2019; D'Croz-Baron et al. 2019, Jia et al. 2019, Lehmann et al. 2005, Musaeus et al. 2019, Nagabhushan Kalburgi et al. 2020, Smailovic et al. 2019, Takarae et al. 2022). The temporal parameters of microstates can be interpreted neurophysiologically and may implicate specific neural system impairments. For instance, a shorter duration of a microstate may reflect premature termination or problem sustaining activities of certain neural generators, and reduced occurrence may indicate difficulty coordinating activities of a specific set of neural generators that give rise to a certain microstate (Khanna et al. 2015). Alterations in transition patterns between microstates may indicate difficulty invoking or over-relying specific encoded sequential activation of neural assemblies (Khanna et al. 2015). Further, variations in the microstate topography could imply subtle structural or functional disturbances within a specific network (Murray et al. 2008; Vaughan 1982).

Temporal parameters of microstates also distinguish between demographic characteristics, such as age and sex (Koenig et al. 2002; Zanesco et al. 2020b). Sex differences may be particularly important when considering FXS because FMRP1 is located on the X chromosome. The inheritance pattern follows the X chromosome linked dominance model, and the affected X chromosome is passed from the mother onto the offspring (Bartholomay et al. 2019). Because females have two X chromosomes, the unaffected X chromosome from the father allows some production of FMRP, and this results in milder symptoms for females with FXS. Accordingly, milder, intermediate level alterations in EEG characteristics have been reported in females (Pedapati et al. 2022; Smith et al. 2021). It is, however, not clear if the milder alteration may have network specificity, affecting only specific microstates.

We present a study of resting EEG microstates in a large sample of individuals with FXS and control participants. We examined group differences in temporal characteristics of EEG microstates and compared microstate topographies and transition patterns. We further examined relations between microstate characteristics and clinical/demographic characteristics, such as IQ and sex. Finally, we examined EEG spectral characteristics to connect our work with prior studies of FXS examining oscillatory properties of resting EEG.

Materials and Methods

Participants

Resting-state EEG data from 141 participants (70 FXS participants (32 females, 38 males) and 71 typically developing control (TDC) participants (30 females, 41 males) were included in this study. The following analyses were performed using publicly available data (https://zenodo.org/record/7149276), and additional data, such as chronological ages, were provided by the research group that conducted the original work. Details regarding recruitment and preprocessing are provided in published work (Pedapati et al. 2022; Smith et al. 2021). Briefly, all FXS participants were recruited through a federally established regional FXS center at a tertiary hospital in the USA and have full-mutation FXS that was confirmed by Southern Blot and PCR analyses (Pedapati et al. 2022; Smith et al. 2021). Only eyes-open resting EEG was collected during passive viewing of a silent movie that was standardized across participants (Pedapati et al. 2022; Smith et al. 2021). Six participants (4 FXS and 2 TDC participants) were excluded from the original sample because of excessive residual artifacts, and two participants (1 FXS and 1 TDC) were excluded because they had less than 2 min of usable data after preprocessing. The remaining 65 participants with FXS and 68 TDC participants were included in the further analysis. Spectral decomposition was performed with the downloaded data before additional preprocessing steps were applied for microstate analysis.

The total duration of the preprocessed data was similar between groups, with means(sd) of 257.88(38.14) and 263.97(30.14) seconds for the FXS and TDC groups respectively, t(120) = 1.01, n.s. Groups did not significantly differ based on chronological age or sex ratio but differed significantly by non-verbal IQs (NVIQ). Table 1 summarizes the clinical and demographic information for FXS and TDC groups.

Microstate Analysis

Topographic clustering was employed to determine the optimal number and configuration of microstate topographies. Procedures and parameters for the first- and second-level clustering closely followed published work (Takarae et al. 2022; Zanesco et al. 2020b, 2021b).

Additional Preprocessing for Microstate Analysis

The downloaded data were low-pass filtered at 40 Hz, and the channel-wise mean of the entire data period was used to demean the signal for each channel. Then, Cartool (Brunet et al. 2011) was used to spatially smooth individual EEG using inter-septile weighted means (Michel et al. 2019).

First-level Clustering

Topographical maps were extracted at peaks of the global field power (GFP) during the first-level clustering using Cartool (Brunet et al. 2011). GFP peaks reflect moments of high neural synchronization, which provides the optimal characterization of the momentary, quasi-stable activation of large-scale networks (Zanesco 2020). Topographical maps at the GFP peaks were then entered into a modified k-means clustering for each participant. The optimal number of clusters was selected through an iterative process using the following method. A subset of k (varied from 1 to 12) maps was randomly selected from all topographical maps in the participant data as initial centroids for clustering. Spatial correlations between the k centroid maps and the remaining maps were computed. The maps were assigned to the centroid with which they had the highest spatial correlation, resulting in k clusters of maps. Maps were not assigned to a centroid if the highest correlation was lower than 0.5. The polarity of the maps was ignored by correcting the sign of the spatial correlation.

After all maps were assigned to a cluster, new centroid maps were created by averaging the constituent maps assigned to the given k clusters. Any remaining maps that were not assigned to a cluster in the prior iteration were compared to the newly computed centroids and assigned again based on the correlation criterion. This process continued iteratively until the global explained variance (GEV) between the average centroids and the maps converged to a limit. For each k (1 to 12), this procedure was repeated 100 times, with a new subset of k centroids selected for each iteration. The optimal number of clusters was determined by a meta-criterion defined by 7 independent criteria (Bréchet et al. 2019; Custo et al. 2017).

Second-level Clustering

Once the first-level clustering was completed for each participant, all clusters from the participants were entered into a second-level clustering, and the second-level clustering resulted in the sample-level, global clusters. A set of k (1

Table 1 Clinical and demographic characteristics of participants included in the microstate analysis

	FXS (n=65)	TDC (n=68)	
Non-verbal IQ	40.05 (36.48)	103.39 (10.67)	t(76) = p < .0001
Chronological age	20.70 (9.8)	22.28 (10.93)	t < 1, n.s.
Percent female	46.15%	39.70%	$\chi^2(1) = 0.33$, n.s.

to 15) maps was randomly selected to use as initial centroids for clustering. As for the first-level clustering, maps were assigned to a centroid only if the correlation to the centroid was greater than 0.5, and the polarity of the maps was ignored. For each level of k, 200 iterations were run, until the GEV converged to a limit. Then, the k centroid solution was selected based on the same meta criterion used in the first-level clustering (Bréchet et al. 2019, Custo et al. 2017).

Fitting

Finally, the global clusters were fitted to the individual EEG data based on spatial correlations between the EEG topography at each time point and global clusters. Each time point in the individual EEG was labeled with the best matching global cluster. This process resulted in a time series of microstates for the participant. Time points that had lower than 0.5 correlations with any of the global clusters were ignored. Microstate segments that were less than 6 samples (~ 24 msec) were ignored, and the time points were split between the preceding and subsequent microstates in the series.

Microstate Parameters and Transition Probabilities

The following parameters were calculated for each microstate for each participant using the microstate time series: global explained variance (GEV), mean duration, occurrence, and mean global field power (GFP). GEV is the percentage of the observed topographic variance of the individual's microstate time series explained by a specific microstate. Mean duration is the average of each occurrence duration of the specific microstate. Occurrence refers to the frequency of occurrence of a specific microstate in events per second. Mean GFP is the normalized average of GFP from the microstate time series that corresponds to the average strength of the electric field for a specific microstate.

The first-order Markov-chain transition probabilities were estimated to examine if there was any increase/decrease in transitions from one specific microstate to another. Cartool was used to calculate the observed transition probabilities as well as the chance probabilities which assumed that all transitions are random. The observed probabilities were first compared to the chance probability via permutation tests using the *coin* package in R with Bonferroni correction. The transition probabilities were further analyzed if the observed probability statistically differed from the chance in at least one of the groups.

The microstates parameters and transition probabilities were analyzed with linear mixed models using the *lme4* package in *R*. Group and microstate type (e.g., microstate topographic configuration A) or transition pairs (e.g., transition

from microstates A to B) were entered as fixed effects, and the model parameters were estimated using maximum likelihood. Random subject intercepts were included in all models to represent between-participant variability. Degrees of freedom were estimated using Satterthwaite approximation, and Type-III tests for fixed effects were performed. Additional pairwise posthoc tests via the *phia* package in *R* were performed for significant effects to aid interpretations where appropriate. Bonferroni correction was used for the post-hoc tests, and there were 15 comparisons for each linear model with temporal parameters. The post-hoc tests for transition probabilities were corrected for 23 comparisons. Correlations between microstate parameters and clinical/demographic variables were also examined with Bonferroni corrections. Because the clinical correlations were examined only for selected microstates (see below), there were 12 correlations in each clinical/demographic domain.

Topographical Analysis

Topographic dissimilarities were compared between groups (FXS vs. TDC) using multivariate distance matrix regression (MDMR) (McArdle et al. 2001, McArtor et al. 2017) with the *MDMR* package in *R* (McArtor 2018). MDMR is a person-centered regression method for estimating statistical associations between multivariate outcomes and categorical or continuous predictors based on dissimilarities among sets of data (McArtor et al. 2017). MDMR has been extended to the mixed-effects modeling framework to account for dependent or hierarchically nested data (McArtor et al. 2017; McArtor 2018).

Topographic dissimilarities between the map centroids from individual-level clustering were quantified by Euclidean distance. The resulting Euclidean distances were compared between groups and microstate types using MDMR. Map topographies were included in the model as nested within individuals when participants had more than one map for a particular microstate type. Analytic p-values are reported for MDMR significance tests (McArtor et al. 2017). A measure of variance among topographies was calculated as the map discrepancy (Studer et al. 2011). Map discrepancy is conceptually akin to a measure of the spatial standard deviation and reflects the average dissimilarity of all topographies within a grouping to the multivariate center of that grouping. A pseudo-R^2 was also estimated based on partitions of sums of squares of dissimilarities based on the fixed effects MDMR model and represents the proportion of total discrepancy among sequences accounted for by covariates.

Relationship to Individual Alpha Power

Previous studies have shown that microstate parameters are strongly correlated with alpha power (Croce et al. 2020), and previous studies of FXS have reported alterations in alpha activity in FXS (Pedapati et al. 2022; Smith et al. 2021; Wang et al. 2017). Thus, our analysis below on spectral characteristics focuses on the alpha band. We first estimated the individual alpha frequency (IAF) by finding the center of gravity in 7–14 Hz to derive the IAF peak, then we set the lower and upper bounds by respectively multiplying the peak by 0.6 and 1.2 (Klimesch 1999; Saggar et al. 2012). Spectral decomposition was performed using *spectopo* function in EEGLAB (Delorme et al. 2004), and IAF power was extracted using the individually set window. IAF peak and power were compared between groups using a t-test with Welch correction for degrees of freedom in *R*. Correlations between microstate temporal parameters and IAF variables were Bonferroni corrected, with 36 correlations each for the IAF peak and power related analyses.

Results

Microstate Parameters

The *k*-means clustering analysis resulted in 6 global clusters, which accounted for 82.60% of the topographic variance. The global clusters are shown in Fig. 1. Our 6 global clusters showed a close resemblance to previous work from our group and others that used the same method and data-driven criteria but used different independent samples (Custo et al. 2017; Takarae et al. 2022; Zanesco et al. 2020b). Following the naming convention in the field, microstates A through D were labeled based on similarities to the classic microstate topographies that have been replicated in previous studies (Koenig et al. 2002, Michel et al. 2018). Microstates E and F were named based on the labels used for these configurations in our prior work (Takarae et al. 2022; Zanesco et al. 2020b). After fitting the global clusters to individual EEG data, the percentages of samples that were assigned the global microstates were similar between

groups, t = 1.41, n.s., means(sd): $M = 79.71\%(10.36)$ for FXS and $M = 82.06\%(8.76)$ for TDC.

In the primary analysis of microstate parameters presented below, the effect of microstate type (A through F) was significant in all the analyses. However, because the primary focus of this study is the differences relating to the FXS diagnosis, we focus on the main effects of group and the interaction between group and microstate type. The effects of microstate type are not discussed in the subsequent text. Means, standard deviations, and standardized effect sizes of group differences on microstate parameters are presented in Tables 2 and 3, respectively.

Global Explained Variance (GEV)

There was no significant overall group difference in GEV, but there was a significant interaction of group and microstate type (Fig. 2), F (5, 798) = 6.71, p < .0001. The interaction effect was driven by greater GEV for microstates C and D in the FXS group compared to the TDC group, whereas GEV was lower for other microstates in the FXS group. The group difference for microstate C was statistically different than microstates A, E, F (p < .01), and B (p < .05) after Bonferroni correction. The group difference for microstate D also significantly differed from microstates A, E (p's < 0.01), and F(p < .05) after Bonferroni correction.

Mean Duration

There was a significant group x microstate type interaction, F(5, 665) = 3.46, p < .01, but no significant main effect of group. The group difference for microstate D was significantly different from those for microstates A and E (p's < 0.05, Bonferroni corrected) (Fig. 3).

Occurrence Per Second

The microstate occurrence did not significantly differ between groups, but there was a significant group by microstate type interaction (Fig. 4), F (5, 665) = 4.62, p < .001. Microstates C and D occurred more frequently in the FXS group than the TDC group, while other microstates were
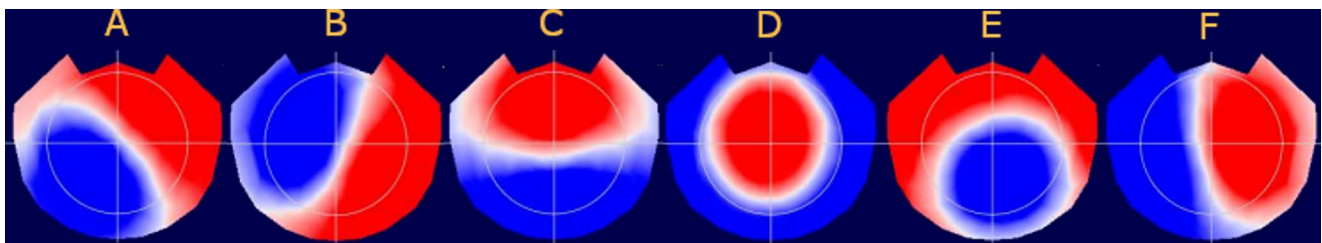
Fig. 1 Voltage scalp maps of the global clusters obtained in the current study. Each map shows the centroid of each cluster. Voltage maps are 2D isometric projections with the nasion oriented towards the top of the map

Table 2 Means and standard deviations for temporal parameters of each microstate by group. Standard deviations are presented in parentheses

	Map A	Map B	Map C	Map D	Map E	Map F
GEV						
FXS	0.06(0.04)	0.05(0.03)	0.19(0.08)	0.11(0.07)	0.09(0.05)	0.04(0.02)
TDC	0.08(0.04)	0.06(0.03)	0.16(0.07)	0.08(0.05)	0.11(0.04)	0.05(0.03)
Mean duration						
FXS	71.67(10.40)	70.86(10.48)	81.26(10.78)	76.90(10.54)	74.62(9.82)	70.50(9.50)
TDC	75.11(8.50)	72.95(9.66)	81.40(11.51)	75.92(10.30)	77.62(9.35)	72.65(9.12)
Occurrence						
FXS	1.15(0.58)	1.07(0.40)	2.35(0.65)	1.76(0.83)	1.61(0.63)	0.87(0.40)
TDC	1.36(0.54)	1.15(0.49)	2.15(0.62)	1.49(0.76)	1.75(0.53)	1.07(0.51)
Mean GFP						
FXS	1.27(0.07)	1.26(0.07)	1.36(0.09)	1.30(0.09)	1.30(0.07)	1.24(0.07)
TDC	1.28(0.07)	1.25(0.08)	1.32(0.09)	1.24(0.07)	1.31(0.08)	1.23(0.07)

Table 3 Standardized effect size d for FXS vs. TDC comparisons for each microstate. Positive values indicate higher values in FXS, and negative values indicate higher values in TDC.

	Map A	Map B	Map C	Map D	Map E	Map F
GEV	-0.42	-0.16	0.42	0.48	-0.30	-0.38
Mean duration	-0.36	-0.21	-0.01	0.09	-0.31	-0.23
Occurrence	-0.39	-0.18	0.32	0.34	-0.26	-0.43
Mean GFP	-0.15	0.12	0.43	0.68	-0.05	0.01

Fig. 2 Global explained variance (GEV) for each microstate by group. Group means and standard errors of the mean are presented. Asterisks indicate significant differences from microstates C (black) or D (light blue)

/ p<.05, **/** p<.01, ***/*** p<.001
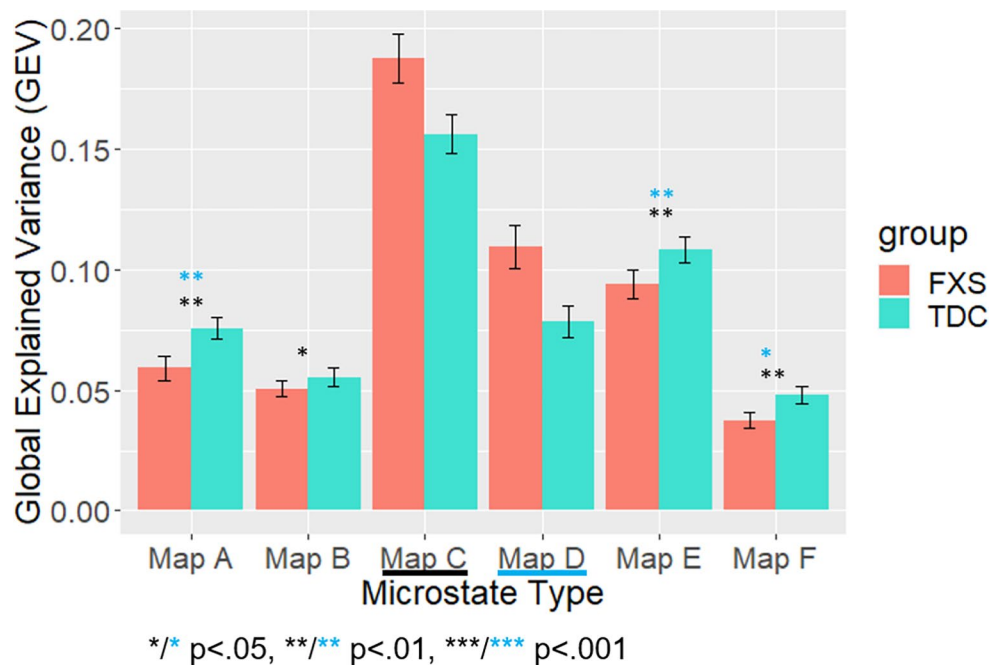
less frequent in the FXS group. The post-hoc comparisons with Bonferroni correction suggest that the group difference in the occurrence of microstate C was statistically different from microstate A (p < .05), and the group difference for microstate D was different from the effects for microstates A (p < .01), E, and F (p's < 0.05).

Mean Global Field Power (GFP)

There was no significant effect of group, but there was a significant group by microstate type interaction (Fig. 5), $F_{(5, 665)} = 8.40$, $p < .0001$. Group differences for the mean GFP were greater for microstates C and D with higher mean GFP for the FXS group, while group differences for other microstates were much smaller. The post-hoc analysis suggested that the group difference for microstate C was significantly different from microstates A (p < .01) and E and F

Fig. 3 Mean duration of each microstate by group. Group means and standard errors of the mean are presented. Asterisks indicate significant differences from microstate D (light blue)
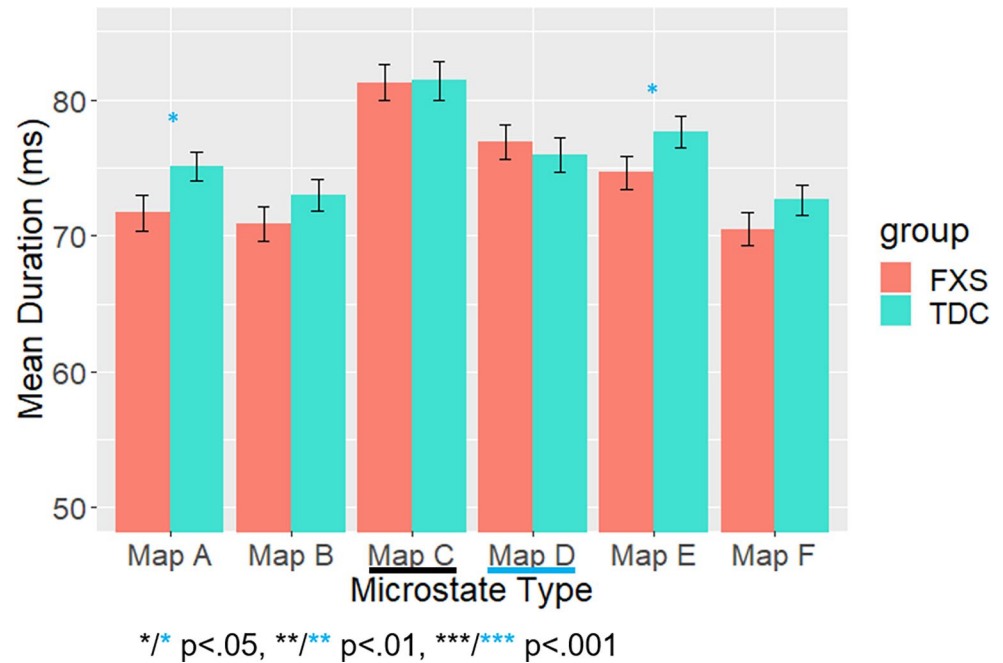
Fig. 4 Occurrence per second for each microstate by group. Group means and standard errors of the mean are presented. Asterisks indicate significant differences from microstates C (black) or D (light blue)
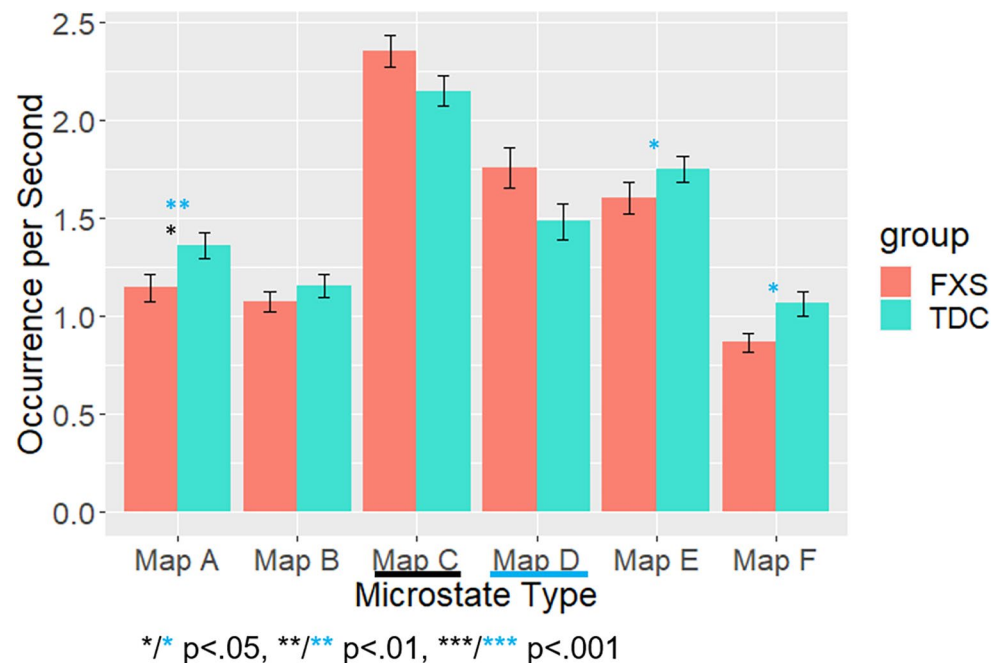
(p's < 0.05). The group difference for microstate D significantly differed from the effects for microstates A, E, and F (p's < 0.001) and B (p < .01).

Transition Probabilities

Although the overall group difference was not significant, the group by transition pairs interaction was significant, $F(22, 2926) = 3.12$, p < .0001. The post-hoc analysis revealed that the group difference in the B to D transition probability was significantly different compared to transitions from A to F (p < .05) after Bonferroni correction. While the B to D transition occurred more frequently in the FXS group (means(sd): $M = 0.13(0.07)$ for FXS and $M = 0.10(0.06)$ for TDC), the A to F transition occurred less frequently in the FXS group than in the TDC group ($M = 0.06(0.04)$ for FXS and $M = 0.08(0.04)$ for TDC).

Topographical Dissimilarity Analysis

MDMR indicated no main effect of group, but a significant interaction between group and microstate ($p < .001$) was

Fig. 5 Mean global field power (GFP) for each microstate by group. Group means and standard errors of the mean are presented. Asterisks indicate significant differences from microstates C (black) or D (light blue)

/ p<.05, **/** p<.01, ***/*** p<.001
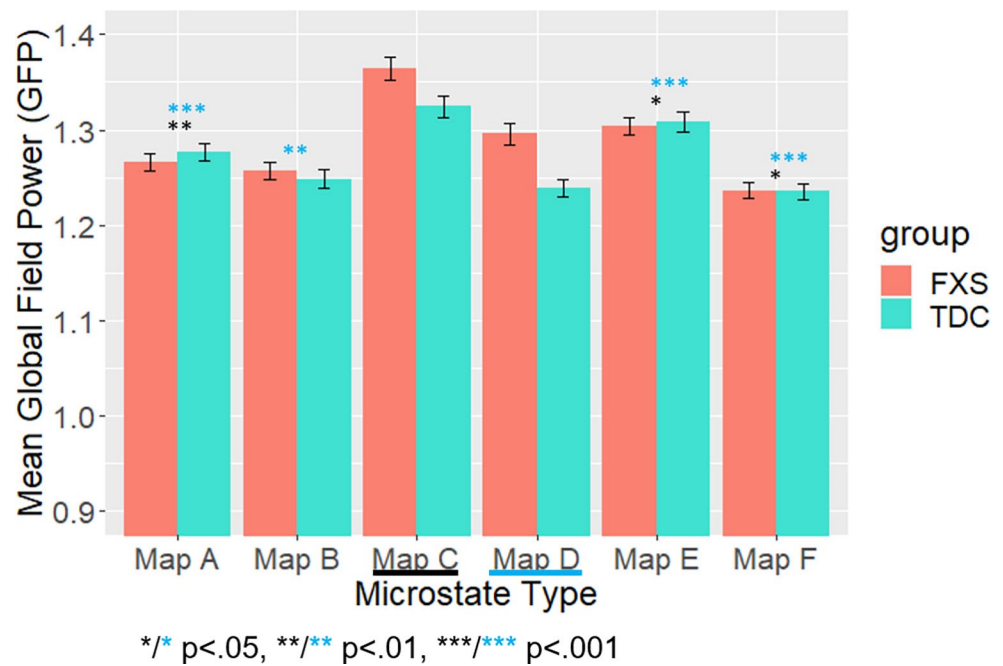
Fig. 6 Symmetrical matrices showing the pairwise Euclidean distances between microstate topographies for microstate B (top left) and D (top right). Pairwise distances between topographies vary from 0 (most similar – blue) to 1 (most dissimilar – red) and are organized by group. The average topographic map for each microstate configuration is shown below each distance matrix as a 2D topographic representation
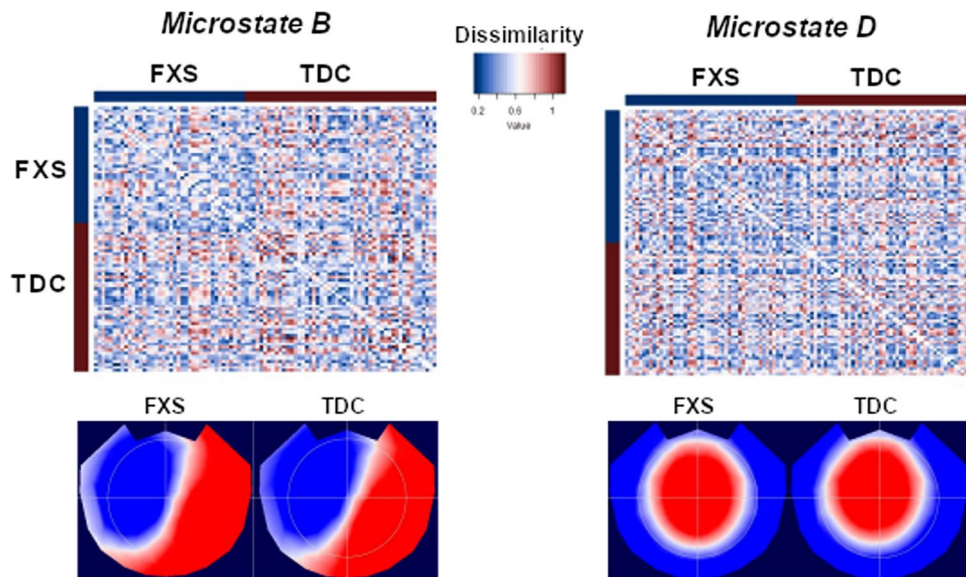
observed. We followed up on this finding by comparing groups for each separate microstate. This process resulted in a significant effect of group for microstate B ($p < .05$), and microstate D ($p < .05$) (Fig. 6), and the analytic p values were confirmed using permutation tests for both microstates with 1,000 permutations each. Group explained 3.01% (pseudo-$R^2 = 0.0301$) of the variance in dissimilarities for topographies in the cluster for microstate B and 3.08% (pseudo-$R^2 = 0.0308$) for microstate D. The relatively low R^2 values suggest that, although statistically significant, there were only minor topographic group differences for both microstates. There was less discrepancy among maps for microstate B for FXS participants (discrepancy = 0.157)

than controls (discrepancy = 0.186). A similar pattern was observed for microstate D with a slightly lower discrepancy in the FXS group (discrepancy = 0.172) than in the TDC group (discrepancy = 0.187). The topographic discrepancy suggests that the microstate configurations were slightly more homogeneous for these microstates among FXS participants than the TDC participants.

Sex Differences

Linear mixed models to examine the effects of group and microstate type were re-run after adding sex as an additional factor. Because of overlaps with the previously presented

2-factor group x microstate type models, we report only the 3-way group by sex by microstate type interaction effect. The 3-way interaction was significant for mean GFP, F(5, 665) = 2.24, p < .05 (Fig. 7A), and there was also a trend toward significance for GEV, F(5, 798) = 2.00, p = .076. Because the trend for GEV is likely to reflect the same functionally related neural system impairments as reflected by differences in mean GFP, only the mean GFP model was further examined. When only male participants were entered

into the group x microstate type model, the group x microstate type interaction effect was significant, F(5, 380) = 8.00, p < .0001 (Fig. 7B). The post-hoc analysis identified significant group differences for microstates C and D (microstate C vs. A (p < .001), B (p < .05), E (p < .001), F (p < .001), and microstate D vs. A (p < .001). E (p < .05), F (p < .05)). The female only model also showed a significant group by microstate type interaction, F(5, 285) = 5.35, p < .001 (Fig. 7B). The post-hoc analysis, however, only indicated significant
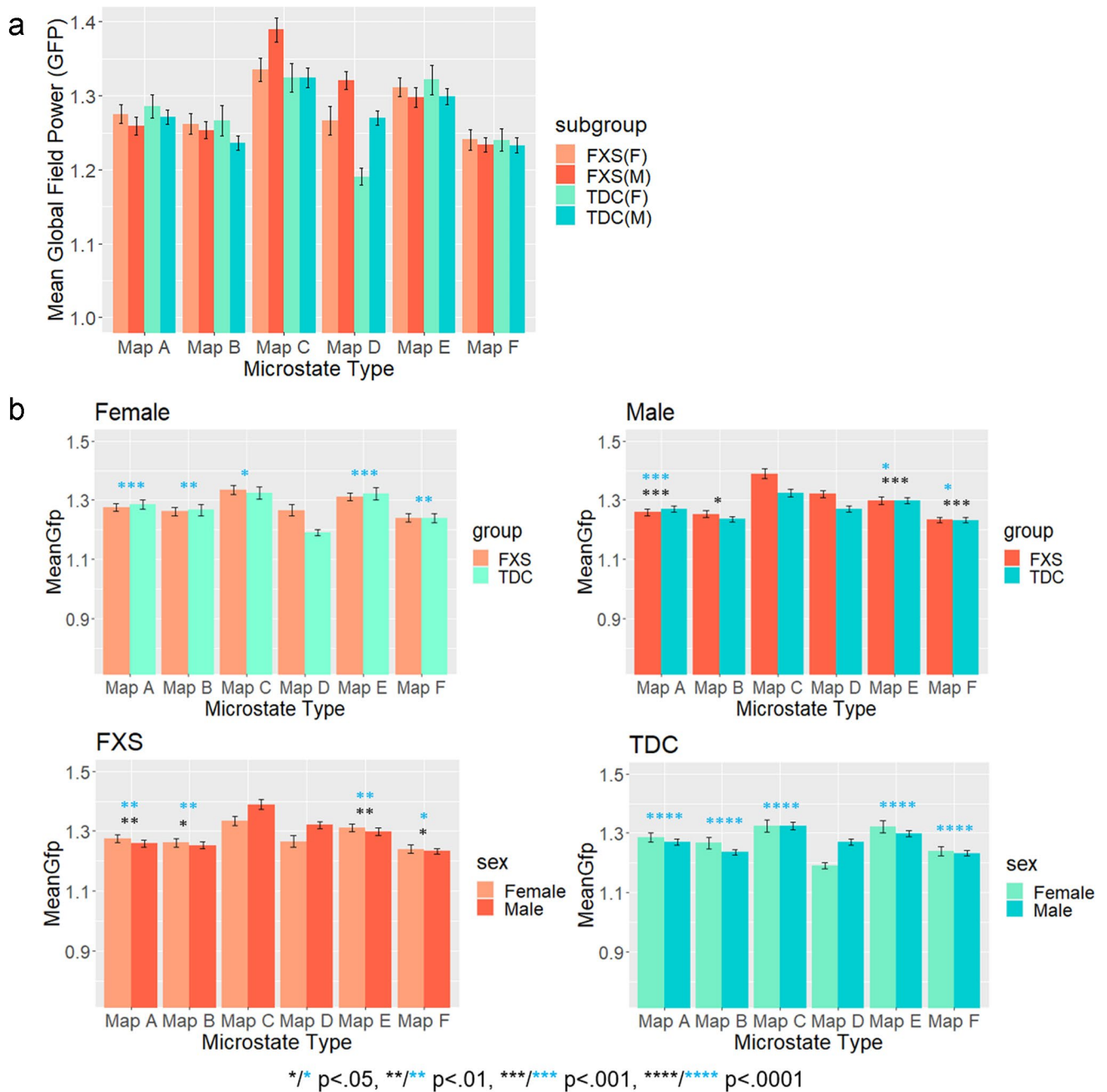
Fig. 7 (A) Mean global field power (GFP) of each microstate by group and sex. Means and standard errors of the mean are presented. **B)** Mean global field power (GFP) of each microstate by group for Female/Male or FXS/TDC participants only. Means and standard errors of the mean are presented. Asterisks indicate significant differences from microstates C (black) or D (light blue)

differences for microstate D compared to other microstates (D vs. A (p < .001), B (p < .01), C (p < .05), E (p < .001), and F (p < .01)). When participants were separated by diagnostic group, the FXS only model showed a significant sex by microstate type interaction (F(5, 325) = 6.84, p < .0001) with the post-hoc tests indicating differences involving microstates C and D (microstate C vs. A (p < .01), B (p < .05), E (p < .01), and F (p < .05), microstate D vs. A (p < .01), B (p < .01), E (p < .01), F (p < .05)). In contrast, the TDC only model showed a significant sex by microstate type interaction (F(5, 340) = 10.96, p < .0001) with post-hoc significant differences involving only microstate D (p's < 0.0001 for differences from all other microstates).

Relationship to Alpha Band Activity

The power spectrum and detailed characteristics of alpha band activities including source estimations have previously been reported using the same sample (Pedapati et al. 2022; Smith et al. 2021). Thus, we only report mean characteristics and focus on relationships to microstate parameters in the current study. Individual alpha frequency (IAF) peaks were lower in the FXS group than in the TDC group, t(129) = 7.24, p < .0001, (means(sd): M = 9.38 Hz (0.44) for FXS and M = 9.91 Hz (0.41) for TDC). The IAF power across all electrodes was significantly higher in the FXS than TDC group, t(130) = 2.78, p < .01 (means(sd): M = 0.65 dB (3.22) for FXS and M = -0.94 dB (3.35) for TDC). We calculated correlations for the mean duration, occurrence, and mean GFP of microstates with individual alpha peak frequency and power (Fig. 8). Correlations involving GEV were not calculated because of the GEV's dependency on other microstate parameters.

Mean microstate duration was longer in individuals with higher IAF peak frequency for most microstates in both groups: A (rho = 0.53, p < .001), B (rho = 0.46, p < .01), C (rho = 0.38, p = .07), E (rho = 0.46, p < .01) and F (rho = 0.50, p < .001) in the FXS group, and B (rho = 0.48, p < .01), D (rho = 0.41, p < .05), E (rho = 0.39, p < .05), and F(rho = 38, p = .06) in the TDC group, after Bonferroni correction. In addition, the occurrence and mean GFP for microstate D were significantly correlated with IAF peak

frequency in the FXS group (rho = -0.47, p < .01 for occurrence and rho = -0.46, p < .01 for mean GFP), but not in the TDC group. Lower IAF peaks were associated with higher mean GFP and more frequent occurrence for microstate D in the FXS group (Fig. 8). No other correlations involving IAF peaks were significant.

Longer mean durations were generally associated with lower amplitude alpha activity: microstates A (rho = -0.58, p < .0001), B (rho = -0.49, p < .01), C (rho = -0.51, p < .001), E (rho = -0.46, p < .01), and F (rho = -0.53, p < .001) in the FXS group, and A (-0.43, p < .05), B (rho = -0.42, p < .05), C (rho = -0.42, p < .05), D (rho = -0.42, p < .05), E (rho = -0.46, p < .01), and F (rhp = -0.41, p < .05) in the TDC group. Additionally, there was a trend toward significance for the occurrence of microstates B (rho = 0.38, p = .053) and F (rho = 0.38, p = .053), only in the TDC group. No other correlations were significant.

Relationship to Other Clinical and Demographic Variables

Because most of the significant group differences in the primary analysis were related to microstates C and D, we correlated their mean duration, occurrence, and mean GFP with NVIQ and age to aid the interpretations of the findings.

NVIQ-related Changes

There was a significant negative correlation between NVIQ scores and the mean GFP of Microstate C, suggesting that lower values of GFP for microstate C are associated with higher NVIQ scores in the FXS group (Spearman's rho = -0.42, p < .05 after Bonferroni correction) (Fig. 9). Other correlations were not significant.

Age-related Changes

Chronological age was positively correlated with the mean duration of microstates C and D in both groups, though the correlations were higher in the TDC group than the FXS group (microstate C: rho = 0.435, p < .01 for FXS group and rho = 0.672, p < .0001 for TDC group, microstate D:

Fig. 8 Scatter plot for the IAF peak frequency with occurrence (left) and mean GFP (right) of microstate D
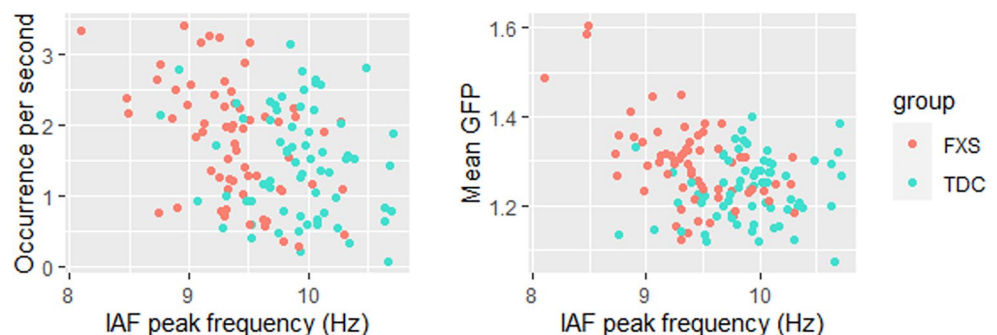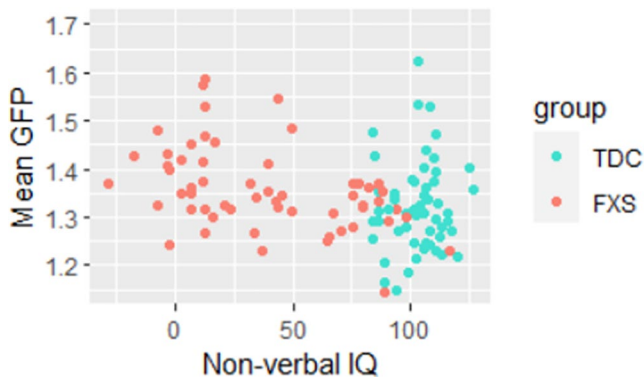
Fig. 9 Scatterplot for the relationship between non-verbal IQ and mean GFP for microstate C

rho = 0.540, p < .0001 for FXS and rho = 0.789, p < .0001 for TDC). Age was also positively correlated with the mean GFP of microstate D in both groups (rho = 0.378, p < .05 for FXS and rho = 0.379, p < .05), but not with microstate C.

Discussion

Despite substantial group differences in functional outcomes (e.g., IQ) between participants with Fragile X syndrome (FXS) and typically developing participants, we did not find large, extensive disruption in the dynamics of all microstates. Rather, group differences were specific to the activity of particular brain circuits each reflecting distinct microstates. We observed significant group by microstate type interactions for GEV, mean duration, occurrence, and mean GFP in a series of linear mixed models. The interaction was driven by group differences in microstate C and D temporal parameters. In addition, transition pattern analysis suggests that the probability of microstates B to D transitions increased in the FXS group compared to the TDC group. Likewise, the topographic configuration of microstates B and D differed between groups, and the topography of microstates B and D was less heterogeneous in the FXS group.

Sex differences between male and female individuals with FXS were also observed for microstates C and D. While past studies have shown sex differences in mean duration and occurrence in certain microstates, including C and D, in typically developing individuals (Bagdasarov et al. 2022; Tomescu et al. 2018; Zanesco et al. 2020b), we did not observe group by sex by microstate type interactions for duration and occurrence, suggesting that sex differences in neurophysiological processes that are related to these parameters may not be strongly influenced by FXS. We, however, observed a significant group by sex by microstate type interaction for mean GFP. While the prior studies investigating sex differences did not include mean GFP

measures, the mean GFP is considered to reflect the degree of neural synchronization among the neural generators of the network, contributing to the overall strength of the scalp electric field (Khanna et al. 2015). Potential excitation to inhibition imbalances in FXS (Nomura 2021; Paluszkiewicz et al. 2011; Pedapati et al. 2022) could affect mean GFP because of the proposed role of inhibition in neural synchronization (Adesnik 2018; Chauhan et al. 2018). Thus, the mean GFP could be sensitive to the severity and degree of neurophysiological alterations within FXS; Certain aspects of the alterations could be associated with sex because of the male-female difference in FMRP production in FXS.

Correlational patterns involving clinical and demographic variables suggest that alterations for microstates C and D may relate to different aspects of cognition in FXS. Microstate C was more prominent in the FXS group than the TDC group, as observed as elevated GEV, occurrence, and mean GFP. The greater mean GFP of microstate C was associated with lower NVIQ scores in FXS. The increase in mean GFP appeared specific to male participants who tend to have more profound intellectual impairments. Intellectual impairments in FXS are highly correlated with FMRP levels (Kim et al. 2019), which are generally lower in males. Thus, the unusually high neural synchronization associated with microstate C may be particularly relevant to the intellectual impairments among FXS. Microstate C has been associated with the default mode network through source localization studies, and default network maturation has been associated with intellectual development in developmental disabilities, including FXS (Hall et al. 2013; Lee et al. 2022).

The unusually high neural synchronization is also reminiscent of the previously reported greater sensory-related ERP amplitude in FXS (Ethridge et al. 2019, Knoth et al. 2012). ERPs are generated via synchronization of neuronal activities in response to sensory stimulation and have strong representations of lower frequency signals (Makeig et al. 2002). The current data add that neural synchronization in lower frequencies may also be increased at rest in FXS within a specific network. In contrast, previous studies have suggested that evoked responses in higher frequency ranges may be reduced in FXS (Ethridge et al. 2017, 2019). Further investigations are needed to clarify frequency specific alterations of neural synchronization in FXS.

Temporal parameters for microstate D showed different patterns of group differences and correlations compared to microstate C. The GEV, mean duration, occurrence, and mean GFP were elevated in the FXS group compared to the TDC group with respect to this microstate. The mean GFP was greater in both male and female FXS participants compared to their TDC counterparts, and the group difference was similar between male and female participants. There was no significant correlation between NVIQ and

microstate D parameters, suggesting that it may not relate to general intellectual disabilities.

Source localization studies have associated microstate D with the frontoparietal attention network (Britz et al. 2010b; Custo et al. 2017), and its parameters change as a function of attention demands in the task and arousal levels (Seitzman et al. 2017). Attention impairments are frequently observed and considered prognostic of FXS (Scerif et al. 2012). While the occurrence of microstate D was overall higher in the FXS group compared to the TDC group, the transition analysis suggests that specific transitions from microstate B to D may contribute to the increased occurrence of microstate D in the FXS group. It appears that engagement of attention control (microstate D) following sensory processing (microstate B) is more critical to perform the resting state task (i.e., passively viewing a silent movie) in the FXS group.

The occurrence and mean GFP of microstate D were significantly correlated with the individual alpha peak frequency. Alpha activities play an essential role in generation of microstates, and early depictions of microstates were conducted using alpha band EEG (Lehmann 1971). Microstate parameters are most strongly correlated with alpha power while the correlations with other frequency bands are much weaker (Croce et al. 2020). It has been shown that the periodicity of microstates occurs twice the alpha frequency (Lehmann 1971; von Wegner et al. 2017) and is associated with the phase of resting alpha oscillations (von Wegner et al. 2021). The thalamus plays a critical role in generating cortical alpha (Halgren et al. 2019), and structural alterations in the thalamus have been reported in FXS. For instance, reduced gray matter density in the thalamus (Hall et al. 2013) and lower fractional anisotropy in regions connecting the thalamus and neocortical regions (Swanson et al. 2018) have been documented. These abnormalities may yield changes in both alpha rhythm and temporal dynamics of microstates in FXS.

While the alpha band is typically defined as 8-12 Hz, its peak frequency is known to vary across individuals. Alpha peak frequencies generally increase from childhood to adolescence (Freschl et al. 2022) then decrease through adulthood (Klimesch 1999). Further, notable shifts in the alpha peak frequency (thalamocortical dysrhythmia) have been reported in several clinical disorders, including epilepsy, tinnitus, and depression (Ridder et al. 2015; Llinás et al. 1999, 2005). In some of these conditions, such as tinnitus, it has been suggested that deafferentation of sensory input reduces the information flow to the thalamus, which results in the slowing of the alpha rhythm (Vanneste et al. 2018). It has been shown that the alpha peak shifts towards the theta frequency in FXS (Van der Molen et al. 2013, Smith et al. 2021) as well as showing more anterior localization (Pedapati et al. 2022). The slowing of the alpha rhythm may

alter optimal temporal windows for inhibitory control over sensory input, which could result in less efficient top-down modulation or increased efforts to achieve such modulation. Though speculative, the aforementioned increased occurrence of B to D transitions may reflect compensation for such inefficiency.

Limitations

One important limitation of the current study is that EEG was only collected during an eyes-open resting condition. Temporal parameters of microstates during eyes-open and -closed could differ (Zanesco et al. 2020b), and previous studies of developmental disabilities have found differences between eyes conditions in EEG microstates (Nagabhushan Kalburgi et al. 2020) and fMRI-based connectivity (Nair et al. 2018). Thus, exploring differences by the eye condition in resting state EEG is an important topic in future research of FXS.

EEG in the current study was recorded while the participant passively viewed a silent movie. Movies are often used to obtain data from young participants or those with developmental disabilities when participants' cooperation is otherwise difficult to obtain. While the microstate topographies observed in the current study closely resemble previously published work, the use of the movie may have affected the relative occurrence, duration, and strength of the signal for each microstate. Likewise, the sensory stimulation of the movie may have interacted with the attentional and intellectual capacities of the participants, influencing patterns of microstate dynamics that are functionally associated with cognition. Thus, the generalization from and to other studies may be limited.

While our sample was relatively large for a study of developmental disabilities, the sample size was not sufficient to perform a detailed characterization of subgroups. Previous studies have reported sex and age differences in microstate parameters, as well as interactions of these demographic variables (Bagdasarov et al. 2022; Koenig et al. 2002; Tomescu et al. 2018; Zanesco et al. 2020b). Investigating these demographic variables is important in the context of X chromosome-linked developmental disabilities. Our sample was, however, not large enough to investigate age-related changes beyond a preliminary check to potentially detect gross changes in developmental trends. The sample was also not sufficient to investigate the potentially complex age-sex relationships. Limited data were also available to examine behavioral and other cognitive correlates to allow deeper insights into the functional relevance of microstates for understanding the pathophysiology of FXS.

Conclusion

Our data showed specific alterations of microstate C and D parameters in FXS participants relative to age-matched TDC participants. Specific alterations in these microstates are potentially related to two of the most prominent cognitive characteristics of FXS: intellectual disabilities and attention impairments. These findings suggest that microstate parameters could serve as clinically relevant markers to investigate cognitive phenotypes and evaluate treatment-related changes. Slowing of the peak IAF and its correlation to microstate D parameters may also suggest changes in the thalamocortical loop in FXS, which may be related to attention control.

Declarations

References

Abreu R, Jorge J, Leal A, Koenig T, Figueiredo P (2020) Eeg microstates predict concurrent fmri dynamic functional connectivity states. Brain Topogr. https://doi.org/10.1007/s10548-020-00805-1

Adesnik H (2018) Layer-specific excitation/inhibition balances during neuronal synchronization in the visual cortex. J Physiol 596(9):1639–1657. https://doi.org/10.1113/jp274986

Al Zoubi O, Mayeli A, Tsuchiyagaito A, Misaki M, Zotev V, Refai H, Paulus M, Bodurka J (2019) Eeg microstates temporal dynamics differentiate individuals with mood and anxiety disorders from healthy subjects. Front Hum Neurosci 13:56. https://doi.org/10.3389/fnhum.2019.00056

Bagdasarov A, Roberts K, Bréchet L, Brunet D, Michel CM, Gaffrey MS (2022) Spatiotemporal dynamics of eeg microstates in four- to eight-year-old children: age- and sex-related effects. Dev Cogn Neurosci 57:101134. https://doi.org/10.1016/j.dcn.2022.101134

Bagni C, Oostra BA (2013) Fragile x syndrome: from protein function to therapy. Am J Med Genet A 161a(11):2809–2821. https://doi.org/10.1002/ajmg.a.36241

Bagni C, Tassone F, Neri G, Hagerman R (2012) Fragile x syndrome: causes, diagnosis, mechanisms, and therapeutics. J Clin Invest 122(12):4314–4322. https://doi.org/10.1172/jci63141

Bartholomay KL, Lee CH, Bruno JL, Lightbody AA, Reiss AL (2019) Closing the gender gap in fragile x syndrome: review on females with fxs and preliminary research findings. Brain Sci 9(1). https://doi.org/10.3390/brainsci9010011

Boyle L, Kaufmann WE (2010) The behavioral phenotype of fmr1 mutations. Am J Med Genet C Semin Med Genet 154c(4):469–476. https://doi.org/10.1002/ajmg.c.30277

Bréchet L, Brunet D, Birot G, Gruetter R, Michel CM, Jorge J (2019) Capturing the spatiotemporal dynamics of self-generated, task-initiated thoughts with eeg and fmri. NeuroImage 194:82–92. https://doi.org/10.1016/j.neuroimage.2019.03.029

Bréchet L, Brunet D, Perogamvros L, Tononi G, Michel CM (2020) Eeg microstates of dreams. Sci Rep 10(1):17069. https://doi.org/10.1038/s41598-020-74075-z

Britz J, Michel CM (2010a) Errors can be related to pre-stimulus differences in erp topography and their concomitant sources. NeuroImage 49(3):2774–2782. https://doi.org/10.1016/j.neuroimage.2009.10.033

Britz J, Van De Ville D, Michel CM (2010b) Bold correlates of eeg topography reveal rapid resting-state network dynamics. NeuroImage 52(4):1162–1170. https://doi.org/10.1016/j.neuroimage.2010.02.052

Britz J, Díaz Hernàndez L, Ro T, Michel CM (2014) Eeg-microstate dependent emergence of perceptual awareness. Front Behav Neurosci 8:163. https://doi.org/10.3389/fnbeh.2014.00163

Brunet D, Murray MM, Michel CM (2011) Spatiotemporal analysis of multichannel eeg: Cartool. Comput Intell Neurosci 2011:813870. https://doi.org/10.1155/2011/813870

Budimirovic DB, Kaufmann WE (2011) What can we learn about autism from studying fragile x syndrome? Dev Neurosci 33(5):379–394. https://doi.org/10.1159/000330213

Chauhan AS, Taylor JD, Nogaret A (2018) Dual mechanism for the emergence of synchronization in inhibitory neural networks. Sci Rep 8(1):11431. https://doi.org/10.1038/s41598-018-29822-8

Comsa IM, Bekinschtein TA, Chennu S (2019) Transient topographical dynamics of the electroencephalogram predict brain connectivity and behavioural responsiveness during drowsiness. Brain Topogr 32(2):315–331. https://doi.org/10.1007/s10548-018-0689-9

Croce P, Quercia A, Costa S, Zappasodi F (2020) Eeg microstates associated with intra- and inter-subject alpha variability. Sci Rep 10(1):2469. https://doi.org/10.1038/s41598-020-58787-w

Custo A, Van De Ville D, Wells WM, Tomescu MI, Brunet D, Michel CM (2017) Electroencephalographic resting-state networks: source localization of microstates. Brain Connect 7(10):671–682. https://doi.org/10.1089/brain.2016.0476

D'Croz-Baron DF, Baker M, Michel CM, Karp T (2019) Eeg microstates analysis in young adults with autism spectrum disorder during resting-state. Front Hum Neurosci 13:173. https://doi.org/10.3389/fnhum.2019.00173

De Ridder D, Vanneste S, Langguth B, Llinas R (2015) Thalamocortical dysrhythmia: a theoretical update in tinnitus. Front Neurol 6:124. https://doi.org/10.3389/fneur.2015.00124

Delorme A, Makeig S (2004) Eeglab: an open source toolbox for analysis of single-trial eeg dynamics including independent component analysis. J Neurosci Methods 134(1):9–21. https://doi.org/10.1016/j.jneumeth.2003.10.009

Ethridge LE, White SP, Mosconi MW, Wang J, Pedapati EV, Erickson CA, Byerly MJ, Sweeney JA (2017) Neural synchronization deficits linked to cortical hyper-excitability and auditory hyper-sensitivity in fragile x syndrome. Mol Autism 8:22. https://doi.org/10.1186/s13229-017-0140-1

Ethridge LE, De Stefano LA, Schmitt LM, Woodruff NE, Brown KL, Tran M, Wang J, Pedapati EV, Erickson CA, Sweeney JA (2019) Auditory eeg biomarkers in fragile x syndrome: clinical relevance. Front Integr Neurosci 13:60. https://doi.org/10.3389/fnint.2019.00060

Freschl J, Azizi LA, Balboa L, Kaldy Z, Blaser E (2022) The development of peak alpha frequency from infancy to adolescence and its role in visual temporal processing: a meta-analysis. Dev Cogn Neurosci 57:101146. https://doi.org/10.1016/j.dcn.2022.101146

Garber KB, Visootsak J, Warren ST (2008) Fragile x syndrome. Eur J Hum Genet 16(6):666–672. https://doi.org/10.1038/ejhg.2008.61

Halgren M, Ulbert I, Bastuji H, Fabó D, Erőss L, Rey M, Devinsky O, Doyle WK, Mak-McCully R, Halgren E, Wittner L, Chauvel P, Heit G, Eskandar E, Mandell A, Cash SS (2019) The generation and propagation of the human alpha rhythm. Proc Natl Acad Sci U S A 116(47):23772–23782. https://doi.org/10.1073/pnas.1913092116

Hall SS, Jiang H, Reiss AL, Greicius MD (2013) Identifying large-scale brain networks in fragile x syndrome. JAMA Psychiatry 70(11):1215–1223. https://doi.org/10.1001/jamapsychiatry.2013.247

Jia H, Yu D (2019) Aberrant intrinsic brain activity in patients with autism spectrum disorder: insights from eeg microstates. Brain Topogr 32(2):295–303. https://doi.org/10.1007/s10548-018-0685-0

Khanna A, Pascual-Leone A, Michel CM, Farzan F (2015) Microstates in resting-state eeg: current status and future directions. Neurosci Biobehav Rev 49:105–113. https://doi.org/10.1016/j.neubiorev.2014.12.010

Kim K, Hessl D, Randol JL, Espinal GM, Schneider A, Protic D, Aydin EY, Hagerman RJ, Hagerman PJ (2019) Association between iq and fmr1 protein (fmrp) across the spectrum of cgg repeat expansions. PLoS ONE 14(12):e0226811. https://doi.org/10.1371/journal.pone.0226811

Klimesch W (1999) Eeg alpha and theta oscillations reflect cognitive and memory performance: a review and analysis. Brain Res Brain Res Rev 29(2–3):169–195. https://doi.org/10.1016/s0165-0173(98)00056-3

Knoth IS, Lippé S (2012) Event-related potential alterations in fragile x syndrome. Front Hum Neurosci 6:264. https://doi.org/10.3389/fnhum.2012.00264

Koenig T, Prichep L, Lehmann D, Sosa PV, Braeker E, Kleinlogel H, Isenhart R, John ER (2002) Millisecond by millisecond, year by year: normative eeg microstates and developmental stages. NeuroImage 16(1):41–48. https://doi.org/10.1006/nimg.2002.1070

Lee JK, Cho ACB, Andrews DS, Ozonoff S, Rogers SJ, Amaral DG, Solomon M, Nordahl CW (2022) Default mode and fronto-parietal network associations with iq development across childhood in autism. J Neurodev Disord 14(1):51. https://doi.org/10.1186/s11689-022-09460-y

Lehmann D (1971) Multichannel topography of human alpha eeg fields. Electroencephalogr Clin Neurophysiol 31(5):439–449. https://doi.org/10.1016/0013-4694(71)90165-9

Lehmann D, Ozaki H, Pal I (1987) Eeg alpha map series: Brain micro-states by space-oriented adaptive segmentation. Electroencephalogr Clin Neurophysiol 67(3):271–288. https://doi.org/10.1016/0013-4694(87)90025-3

Lehmann D, Strik WK, Henggeler B, Koenig T, Koukkou M (1998) Brain electric microstates and momentary conscious mind states as building blocks of spontaneous thinking: I. Visual imagery and abstract thoughts. Int J Psychophysiol 29(1):1–11. https://doi.org/10.1016/s0167-8760(97)00098-6

Lehmann D, Faber PL, Galderisi S, Herrmann WM, Kinoshita T, Koukkou M, Mucci A, Pascual-Marqui RD, Saito N, Wackermann J, Winterer G, Koenig T (2005) Eeg microstate duration and syntax in acute, medication-naive, first-episode schizophrenia: a multi-center study. Psychiatry Res 138(2):141–156. https://doi.org/10.1016/j.pscychresns.2004.05.007

Lehmann D, Pascual-Marqui RD, Strik WK, Koenig T (2010) Core networks for visual-concrete and abstract thought content: a

brain electric microstate analysis. NeuroImage 49(1):1073–1079. https://doi.org/10.1016/j.neuroimage.2009.07.054

Llinás R, Ribary U, Jeanmonod D, Kronberg E, Mitra PP (1999) Thalamocortical dysrhythmia: a neurological and neuropsychiatric syndrome characterized by magnetoencephalography. Proc Natl Acad Sci U S A 96(26):15222–15227. https://doi.org/10.1073/pnas.96.26.15222

Llinás R, Urbano FJ, Leznik E, Ramírez RR, van Marle HJ (2005) Rhythmic and dysrhythmic thalamocortical dynamics: Gaba systems and the edge effect. Trends Neurosci 28(6):325–333. https://doi.org/10.1016/j.tins.2005.04.006

Makeig S, Westerfield M, Jung TP, Enghoff S, Townsend J, Courchesne E, Sejnowski TJ (2002) Dynamic brain sources of visual evoked responses. Science 295(5555):690–694. https://doi.org/10.1126/science.1066168

McArdle BH, Anderson MJ (2001) Fitting multivariate models to community data: a comment on distance-based redundancy analysis. Ecology 82(1):290–297. https://doi.org/10.1890/0012-9658(2001)082[0290:FMMTCD]2.0.CO;2

McArtor DB (2018) Mdmr: Multivariate distance matrix regression. R package version 0.5.1. https://CRAN.R-project.org/package=MDMR

McArtor DB, Lubke GH, Bergeman CS (2017) Extending multivariate distance matrix regression with an effect size measure and the asymptotic null distribution of the test statistic. Psychometrika 82(4):1052–1077. https://doi.org/10.1007/s11336-016-9527-8

Michel CM, Brunet D (2019) Eeg source imaging: a practical review of the analysis steps. Front Neurol 10:325. https://doi.org/10.3389/fneur.2019.00325

Michel CM, Koenig T (2018) Eeg microstates as a tool for studying the temporal dynamics of whole-brain neuronal networks: a review. Neuroimage 180(Pt B 577–593. https://doi.org/10.1016/j.neuroimage.2017.11.062

Milz P, Faber PL, Lehmann D, Koenig T, Kochi K, Pascual-Marqui RD (2016) The functional significance of eeg microstates–associations with modalities of thinking. NeuroImage 125:643–656. https://doi.org/10.1016/j.neuroimage.2015.08.023

Murray MM, Brunet D, Michel CM (2008) Topographic erp analyses: a step-by-step tutorial review. Brain Topogr 20(4):249–264. https://doi.org/10.1007/s10548-008-0054-5

Musaeus CS, Nielsen MS, Høgh P (2019) Microstates as disease and progression markers in patients with mild cognitive impairment. Front Neurosci 13:563. https://doi.org/10.3389/fnins.2019.00563

Musso F, Brinkmeyer J, Mobascher A, Warbrick T, Winterer G (2010) Spontaneous brain activity and eeg microstates. A novel eeg/fmri analysis approach to explore resting-state networks. NeuroImage 52(4):1149–1161. https://doi.org/10.1016/j.neuroimage.2010.01.093

Nagabhushan Kalburgi S, Whitten AP, Key AP, Bodfish JW (2020) Children with autism produce a unique pattern of eeg microstates during an eyes closed resting-state condition. Front Hum Neurosci 14:288. https://doi.org/10.3389/fnhum.2020.00288

Nair S, Jao Keehn RJ, Berkebile MM, Maximo JO, Witkowska N, Müller RA (2018) Local resting state functional connectivity in autism: site and cohort variability and the effect of eye status. Brain Imaging Behav 12(1):168–179. https://doi.org/10.1007/s11682-017-9678-y

Nomura T (2021) Interneuron dysfunction and inhibitory deficits in autism and fragile x syndrome. Cells 10(10). https://doi.org/10.3390/cells10102610

Paluszkiewicz SM, Olmos-Serrano JL, Corbin JG, Huntsman MM (2011) Impaired inhibitory control of cortical synchronization in fragile x syndrome. J Neurophysiol 106(5):2264–2272. https://doi.org/10.1152/jn.00421.2011

Pedapati EV, Schmitt LM, Ethridge LE, Miyakoshi M, Sweeney JA, Liu R, Smith E, Shaffer RC, Dominick KC, Gilbert DL, Wu SW,

Horn PS, Binder DK, Lamy M, Axford M, Erickson CA (2022) Neocortical localization and thalamocortical modulation of neuronal hyperexcitability contribute to fragile x syndrome. Commun Biol 5(1):442. https://doi.org/10.1038/s42003-022-03395-9

Pipinis E, Melynyte S, Koenig T, Jarutyte L, Linkenkaer-Hansen K, Ruksenas O, Griskova-Bulanova I (2017) Association between resting-state microstates and ratings on the amsterdam resting-state questionnaire. Brain Topogr 30(2):245–248. https://doi.org/10.1007/s10548-016-0522-2

Saggar M, King BG, Zanesco AP, Maclean KA, Aichele SR, Jacobs TL, Bridwell DA, Shaver PR, Rosenberg EL, Sahdra BK, Ferrer E, Tang AC, Mangun GR, Wallace BA, Miikkulainen R, Saron CD (2012) Intensive training induces longitudinal changes in meditation state-related eeg oscillatory activity. Front Hum Neurosci 6:256. https://doi.org/10.3389/fnhum.2012.00256

Sansone SM, Schneider A, Bickel E, Berry-Kravis E, Prescott C, Hessl D (2014) Improving iq measurement in intellectual disabilities using true deviation from population norms. J Neurodev Disord 6(1):16. https://doi.org/10.1186/1866-1955-6-16

Scerif G, Longhi E, Cole V, Karmiloff-Smith A, Cornish K (2012) Attention across modalities as a longitudinal predictor of early outcomes: the case of fragile x syndrome. J Child Psychol Psychiatry 53(6):641–650. https://doi.org/10.1111/j.1469-7610.2011.02515.x

Seitzman BA, Abell M, Bartley SC, Erickson MA, Bolbecker AR, Hetrick WP (2017) Cognitive manipulation of brain electric microstates. NeuroImage 146:533–543. https://doi.org/10.1016/j.neuroimage.2016.10.002

Smailovic U, Koenig T, Laukka EJ, Kalpouzos G, Andersson T, Winblad B, Jelic V (2019) Eeg time signature in alzheimer´s disease: functional brain networks falling apart. Neuroimage Clin 24:102046. https://doi.org/10.1016/j.nicl.2019.102046

Smith EG, Pedapati EV, Liu R, Schmitt LM, Dominick KC, Shaffer RC, Sweeney JA, Erickson CA (2021) Sex differences in resting eeg power in fragile x syndrome. J Psychiatr Res 138:89–95. https://doi.org/10.1016/j.jpsychires.2021.03.057

Studer M, Ritschard G, Gabadinho A, Müller NS (2011) Discrepancy analysis of state sequences. Sociol Methods Res 40(3):471–510. https://doi.org/10.1177/0049124111415372

Swanson MR, Wolff JJ, Shen MD, Styner M, Estes A, Gerig G, McKinstry RC, Botteron KN, Piven J, Hazlett HC (2018) Development of white matter circuitry in infants with fragile x syndrome. JAMA Psychiatry 75(5):505–513. https://doi.org/10.1001/jamapsychiatry.2018.0180

Takarae Y, Zanesco A, Keehn B, Chukoskie L, Müller RA, Townsend J (2022) Eeg microstates suggest atypical resting-state network activity in high-functioning children and adolescents with autism spectrum development. Dev Sci 25(4):e13231. https://doi.org/10.1111/desc.13231

Tomescu MI, Rihs TA, Rochas V, Hardmeier M, Britz J, Allali G, Fuhr P, Eliez S, Michel CM (2018) From swing to cane: sex differences of eeg resting-state temporal patterns during maturation and aging. Dev Cogn Neurosci 31:58–66. https://doi.org/10.1016/j.dcn.2018.04.011

Van der Molen MJ, Van der Molen MW (2013) Reduced alpha and exaggerated theta power during the resting-state eeg in fragile x syndrome. Biol Psychol 92(2):216–219. https://doi.org/10.1016/j.biopsycho.2012.11.013

Vanneste S, Song JJ, De Ridder D (2018) Thalamocortical dysrhythmia detected by machine learning. Nat Commun 9(1):1103. https://doi.org/10.1038/s41467-018-02820-0

Vaughan HG Jr. (1982) The neural origins of human event-related potentials. Ann N Y Acad Sci 388:125–138. https://doi.org/10.1111/j.1749-6632.1982.tb50788.x

Verkerk AJ, Pieretti M, Sutcliffe JS, Fu YH, Kuhl DP, Pizzuti A, Reiner O, Richards S, Victoria MF, Zhang FP et al (1991) Identification of a gene (fmr-1) containing a cgg repeat coincident with a breakpoint cluster region exhibiting length variation in fragile x syndrome. Cell 65(5):905–914. https://doi.org/10.1016/0092-8674(91)90397-h

von Wegner F, Tagliazucchi E, Laufs H (2017) Information-theoretical analysis of resting state eeg microstate sequences - non-markovianity, non-stationarity and periodicities. NeuroImage 158:99–111. https://doi.org/10.1016/j.neuroimage.2017.06.062

von Wegner F, Bauer S, Rosenow F, Triesch J, Laufs H (2021) Eeg microstate periodicity explained by rotating phase patterns of resting-state alpha oscillations. NeuroImage 224:117372. https://doi.org/10.1016/j.neuroimage.2020.117372

Wang J, Ethridge LE, Mosconi MW, White SP, Binder DK, Pedapati EV, Erickson CA, Byerly MJ, Sweeney JA (2017) A resting eeg study of neocortical hyperexcitability and altered functional connectivity in fragile x syndrome. J Neurodev Disord 9:11. https://doi.org/10.1186/s11689-017-9191-z

Yuan H, Zotev V, Phillips R, Drevets WC, Bodurka J (2012) Spatiotemporal dynamics of the brain at rest–exploring eeg microstates as electrophysiological signatures of bold resting state networks. NeuroImage 60(4):2062–2072. https://doi.org/10.1016/j.neuroimage.2012.02.031

Zanesco AP (2020) Eeg electric field topography is stable during moments of high field strength. Brain Topogr 33(4):450–460. https://doi.org/10.1007/s10548-020-00780-7

Zanesco AP, Denkova E, Jha AP (2020a) Self-reported mind wandering and response time variability differentiate prestimulus electroencephalogram microstate dynamics during a sustained attention task. J Cogn Neurosci 1–18. https://doi.org/10.1162/jocn_a_01636

Zanesco AP, King BG, Skwara AC, Saron CD (2020b) Within and between-person correlates of the temporal dynamics of resting eeg microstates. NeuroImage 211:116631. https://doi.org/10.1016/j.neuroimage.2020.116631

Zanesco AP, Denkova E, Jha AP (2021a) Associations between self-reported spontaneous thought and temporal sequences of eeg microstates. Brain Cogn 150:105696. https://doi.org/10.1016/j.bandc.2021.105696

Zanesco AP, Skwara AC, King BG, Powers C, Wineberg K, Saron CD (2021b) Meditation training modulates brain electric microstates and felt states of awareness. Hum Brain Mapp. https://doi.org/10.1002/hbm.25430